Base composition at the start of the coding sequence controls the balance between translation initiation and mRNA degradation in *E. coli*.

Anna Lipońska[1*], Laura Monlezun[1], Isaac Wilkins[2], Saravuth Ngo[1], Thomas Oïffer[1], Cylia Bouchachi[1], John F. Hunt[3], Daniel P. Aalberts[2†] and Grégory Boël[1†].

[1]UMR 8261, CNRS, Université Paris Cité, Institut de Biologie Physico-Chimique, 13 rue Pierre et Marie Curie, 75005 Paris, France. [2]Physics Department, Williams College, Williamstown, MA 01267, USA. [3]Department of Biological Sciences, Columbia University, New York, NY 10027, USA

[*] Current address: Department of Microbiology-Immunology, Northwestern University Feinberg School of Medicine, 320 E Superior St, Chicago, IL 60611.

[†] To whom correspondence may be addressed:
GB, Mailing address: Institut de Biologie Physico-Chimique, 13 rue Pierre et Marie Curie, 75005 Paris, France; Phone: +33-1-58415121; E-mail: boel@ibpc.fr.
DPA, Mailing address: Physics Department, Williams College, Williamstown, MA 01267, USA; Phone: (413)-597-3520; E-mail: aalberts@williams.edu.

Abstract

Protein synthesis efficiency is highly dependent on mRNA coding sequence. Furthermore, there is extensive evidence of a correlation between mRNA stability and protein expression level, though the mechanistic determinants remain unclear. Using yellow fluorescent protein (YFP) as a reporter gene, we herein demonstrate that adenosine (A) abundance in the first six codons is a critical determinant for achieving high protein synthesis in *E. coli*. Increasing A and/or decreasing guanosine (G) content in this region results in substantial increases in protein expression level both *in vivo* and *in vitro* that are correlated with steady-state mRNA concentration *in vivo*, and this effect is attributable to changes in the stability of the mRNA that are directly coupled to its translation efficiency. Increasing A content promotes mRNA incorporation into the functional 70S ribosomal initiation complex without altering its affinity for the 30S ribosomal subunit. These results support a model in which base composition in the first six codons modulates local mRNA folding energy to control the balance between productive translation initiation *versus* degradation of mRNAs bound to the 30S ribosomal subunit. Based on these findings, we developed a short N-terminal coding sequence that optimizes translation initiation efficiency for protein production in *E. coli*.

Introduction

Biologcial protein synthesis comprises the translation by the ribosome of mRNA into protein. Since the genetic code uses 61 nucleotide codons to encode the 20 amino acids contained in proteins, there is a degeneracy that allows a large number of mRNA sequences with different codon usages to encode the same protein sequence. Nevertheless, synonymous sequences can strongly affect protein expression (1-8). The mechanisms behind this effect remain unclear in part because synonymous codons can influence translation in different ways. First, they change the base composition and therefore the structure of the mRNA. Secondly, they can use different tRNA with different abundance or affinity.

Several studies have shown that codons can change translation efficiency during elongation of the nascent protein (4,9-16). It has been widely believed that tRNA abundance, which is correlated with *Escherichia coli* codon usage (6,10,17), controls translation elongation efficiency (1,4,6,7,9,10,18-20). This model postulates that the so-called rare codons can slow ribosome elongation, but recent publications have challenged this view (11,15,16,21-33). Ribosome profiling and high throughput protein expression experiments have established that translation elongation efficiency can vary, but there only a weak correlation with tRNA abundance (13,15,16,23,34-36). Moreover, these studies have shown that codons influence mRNA translation and that there is a correlation with the translation of mRNA and mRNA stability (13,37-41), possibly related to ribosomal stalling and collision (42,43).

However, for most mRNA the rate-limiting step of protein synthesis is the formation of a 70S elongation-competent complex (70S EC) a mature form of the 70S initiation complex (70S IC) (44-46). The rate of 70S EC formation depends on the mRNA and ranges between 0.5 sec to a few seconds (45,47,48), while translation elongation occurs faster at an average speed of 20 to 24 amino acids per second (49,50). The current general model of 70S IC assembly starts with the formation of the 30S pre-IC, which is constructed by the three initiation factors (IF1, 2, and 3), the initiator tRNA (fMet-tRNA^{fMet}) and the 30S ribosomal subunit (51). This complex then associates with the mRNA at the initiation codon, which, in most cases in *E. coli*, is guided by the Shine-Dalgarno sequence (SD) upstream of this codon and by the nucleotide composition of the surrounding region (17,52). Finally, joining of the 50S ribosomal subunit triggers IF-3 dissociation to form the 70S pre-IC, where the repositioning of

fMet-tRNA^{fMet} and departure of IF1 create the 70S IC. Subsequent dissociation of IF2 generates the 70S EC (45,51). The duration of each of these steps determines the effective translation initiation rate (TIR).

TIR also determines the density of ribosomes on the mRNA, thus influencing ribosome stalling (53). It has been proposed that the collision of a stalled ribosome by a trailing ribosome stimulates abortive termination of the stalled ribosome and this effect is dependent on the TIR (54). The TIR can be modulated by the folding of the sequence upstream the initiating codon (5'UTR) which can mask the SD or/and the initiating codon (21,34,55-58). Furthermore, mRNA folding extending 40 nucleotides into the coding sequence can also influence TIR (13,21). The mRNA secondary structures formed in this region can be modified by environmental conditions like temperature or interaction with *trans*-acting regulators, small RNA, or ribosomes in order to regulate protein expression (59). The SD can also modulate the formation of the initiation complex by its complementarity with the anti-SD sequence of the 16S rRNA and its position in the sequence (60-63).

In the region of the mRNA surrounding the ATG several studies have shown that nucleotide base biases toward Adenosine (A) correlates with an increase in protein expression (52,64,65). We additionally found that guanosine (G) in the first 18 nucleotides of the coding sequence reduces protein expression (13,66). Bias in nucleotide base composition is clearly observed in this region of protein coding sequences in the *E. coli* K12 genome (**Supplementary Figure S1**). This small region has been proposed to control binding to the 30S pre-IC via ribosomal protein S1 (67,68) in order to form the 30S IC, which is an essential precursor to formation of the functional 70S IC. This mRNA region has furthermore been implicated in guiding alignment of the ribosome at the proper initiation codon (52). Several studies have shown a preponderant role of the first codons in translation, some of them suggesting that rare codons favor expression (11,69), but this effect seems likely to be attributable to base composition because these codons are enriched in A/U *versus* G/C (17). A recent study suggested that the identity of amino acid encoded by codons 3-5 can enhance protein synthesis by preventing pausing of the ribosome and premature termination of protein synthesis (70). This study demonstrated that having Lys at position 3 is particularly effective at promoting protein expression. However, Lys is encoded by A-rich codons (AAA and AAG), and the inability to change aa identity

without changing the nucleotides in the codon make it fundamentally difficult to distinguish aa *versus* codon effects.

In the work presented here, we employ a Yellow Fluorescence Protein (YFP) reporter gene to characterize the influence of the nucleotide base composition in first six codons. We modify the A and G fractions in this region either via synonymous codon substitutions or by appending the reporter to the first 21 nucleotides from a very highly-expressed endogenous *E. coli* gene. Fluorescence measurements show that increasing A content or decreasing G content produces up to 10-fold increases in expression of the YFP reporter. In all the reporters studied, improvement in protein expression result in an increase of the mRNA stability. We furthermore show that the 5' coding sequence that produces the greatest increase in YFP expression, which we named "Translation Boosting Tag" (TBT), strongly enhances expression of poorly expressed proteins when fused in front of their coding sequences in a T7 expression system. Finally, we present biochemical studies demonstrating that modulating A and G content in first six codons at the 5' end of the coding sequence does not change mRNA affinity for the 30S ribosomal subunit, but it does change the efficiency with which that complex progresses to form a productive 70S IC. These results suggest that the formation of the 70S IC from the 30S IC controls a competition between translation initiation and mRNA decay that coordinates these two processes based on the nucleotide base content in the ribosome-docking region at the start of the coding sequence. We propose that this mechanism is a central feature of mRNA metabolism in *E. coli* that optimizes the use of metabolic resources by initiating mRNA decay upstream of translating ribosomes rather than downstream where decay would lead to wasting the energy used to synthesize incomplete proteins.

Materials and Methods

Plasmid and strains – *E. coli* strain DH5α (71) was used for plasmid constructions. All experiment with a use of pMMB67EH plasmids (72) were performed in MG1655 *E. coli* strain (73). Proteins overexpression with pET21 plasmids were carried out in *E. coli* strain BL21 (DE3) (74). Cultures were grown at 37 °C in Luria-Bertani Miller broth (LB-Difco) supplemented with ampicillin at 100 µg/ml. Plasmids were constructed by PCR amplification of the whole plasmids with the CloneAmp Hifi polymerase (Takara)

and assembly of the insert part with the NEBuilder HiFi DNA Assembly kit. The *yfp* variants plasmids were constructed by amplification of the pMMB67EH (72) backbone with primers and amplification of the *yfp* gene (75,76) with primers that contain or not the modification of the first codon of the *yfp* or that add the different TBT sequences, the primers are described in **Table 1**. The same approach was used to insert the TBT sequence in the pET21 expressed test genes *ycaQ*, RSP_2139, SCO1897 and SRU_1983 that we have used in our previous study (13). A 38nt RNA malachite green aptamer (MGapt) was added as described by Siegal-Gaskins *et al.*, (77) in the 3'UTR of the reporter mRNA, 10nt downstream of the stop codon of the TBT or TBT_G *yfp* genes. To that end, a PCR amplification of the whole plasmids was performed with primers H070 and H071 which contain 20 bases of homology to allow plasmid recircularization using the NEBuilder HiFi DNA Assembly kit.

Drop assay – Samples corresponding to OD_{600}=1 of bacterial overnight cultures were centrifuged and diluted in 1 ml LB from which further dilutions were prepared: 10^{-1}, 10^{-2}, 10^{-3}, 10^{-4}, 10^{-5}. 5 µl of sample was placed on LB ampicillin (100 µg/ml) plate and grown O/N at 37 °C. Fluorescence was measured using Typhoon FLA 9 500 apparatus at 473 nm, using BPB1 filter. The results for the best dilution are presented in the figures. Experiments were repeated 3 times.

***In vivo* measures of YFP and TBT variants –** Bacteria were grown in Falcon 96-well sterile plate in CLARIOstar (BMG LabTech) device to quantify optic density of bacteria and the emission of YFP fluorescence (ex 497-15/em 540-20 gain 1000, measured from top 4.0 diameter every 30 min). 2 µl of overnight culture was added directly to 200µl of LB ampicillin (100 µg/ml) (without or with 1 mM IPTG), 60µl of mineral oil (Sigma Life Science) was added to prevent evaporation of the medium and to keep sterile conditions. Each culture was made in triplicate. Data were analyzed with Prism 7 software.

For the experience with samples collection for northern and western blot, bacteria were grown at 37 °C until OD_{600}=0.5, then 1 mM IPTG was added. The samples were collected at 0, 10, 60 and 120 min. For protein sample an equivalent sample for 1 OD sample was collected and centrifuged, the pellets were resuspended in 200 µl of 1x Laemmli sample buffer (Bio-Rad) and boiled for 2 min at 95°C before migration on SDS denaturing gel. For the RNA sample a 1 ml of culture were collected and centrifuged

and resuspended in 150 µl of RNAsnap (78) and processed as described for the RNAsnap procedure. Samples were analyzed on a 12.5% SDS-PAGE gel, by western blot and on agarose gel by northern blot.

Test genes – Plasmids encoding genes *ycaQ* (*E. coli*), RSP_2139 (*Rhodobacter sphaeroides*), SCO1897 (*Streptomyces coelicolor*) and SRU_1983 (*Salinibacter ruber*) were previously assessed for their expression in the *E. coli* Bl21 DE3 strain (13). We introduced the TBT sequence in the 5'-end of the coding sequence (see above). Then all the constructs with or without the TBT sequence were grown at 37 °C to OD_{600}=0.5 in LB with Amp 100 µg/ml. Protein expression was induced by addition of 1 mM IPTG for 16h at 17 °C. Samples of 1 OD were collected before and after induction and analyzed on gel on a 12.5% SDS-PAGE gel and by western blot.

Western Blot – Equal amounts of Total Protein extracts were migrated on a 12.5% SDS-PAGE gel and transferred onto Immun-Blot PVDF blotting membrane (Bio-Rad). Transfer was performed with the Bio-Rad Transfer System (30 min, 25V). For YFP detection, an anti-GFP polyclonal antibody was used (Invitrogen, 11122) in dilution 1:1000 in 1X PBS, 0.1 % Tween-20 and detected with an anti-rabbit IRdye 800CW (LI-COR, 926-32213) in dilution 1:20 000 in the same buffer. For proteins with his-tag we used anti-6xHis-tag primary antibody (Covalab, ref. HIS.HS/ EH158) in dilution 1:2 000 detected with anti-mouse IRdye 800CW (LI-COR, 926-32210) in dilution 1:20 000. The membrane was visualized with Odyssey scanner (LI-COR).

mRNA stability test – Bacteria were grown until OD_{600}= 0.5, where the 1 mM IPTG was added. Induction was carried out for 10 min and was stopped by adding of rifampicin (0.5 mg/ml; 0.6 mM). Samples were collected as indicated after 1, 2, 3 and 4 minutes; to stop cell growth 10 mM sodium azide was added. The mixture was vortexed and centrifuged (1 min/ RT/ 16 000 x g) and RNA were isolated with the RNAsnap method(78).

***In vitro* transcription –** The DNA templates used to generate mRNAs for *in vitro* translation assays were PCR amplified with primers C034 and C035 from the corresponding pMMB67EH plasmids. The forward primer contains the T7 polymerase promoter sequence (5'-GCGAATTAATACGACTCACTATAGGG-3'). *In vitro* mRNA

synthesis was then carried out at 37 °C for 4 h in T7 RiboMAX Large Scale RNA Production System kit (Promega) according to the manufacturer's recommendations. At the end of the reaction, DNA templates were degraded by adding DNAse I for 15 min and the mRNA transcripts were purified using TRIzol Reagent (Thermo Fisher Scientific) and Direct-zol RNA Miniprep kit (Zymo Research). The mRNAs were finally eluted in The RNA Storage Solution (Ambion, Thermo Fisher Scientific) and stored at -80 °C.

***In vitro* translation –** To test the expression of the different constructs, 1.4 µM of each purified mRNA was used in PURExpress *in vitro* Protein Synthesis Kit (NEB#E6800) in 10 µl reaction in 384 well Small Volume black plate (Grenier 788 096). Fluorescence was measured with CLARIOstar (BMG LabTech; ex 497-15/em 540-20 gain 1000, measure every 4 min) during 4 hours at 37 °C. After reaction 2 µl of reaction was stopped with 4x Laemmli sample buffer (Bio-Rad) and used for western blot analysis.
For the IVTA separated on sucrose gradient (**Figure 4B**) reactions were performed in a final volume of 100 µl using the PURExpress ΔRibosome *In vitro* Protein Synthesis Kit (New England Biolabs) according to the manufacturer instructions and with ribosomes purified from *E. coli* strain MRE600(79) at a final concentration of 2 µM. The reporter mRNA was added at a final concentration of 1 µM and the reaction was then carried out at 37 °C for 1h. The translation of the reporter mRNA was monitored every 2 min by measuring YFP fluorescence was measured on a CLARIOstar plate reader (BMG Labtech).

Polysomes fractionation on sucrose gradient and RNA precipitation – The entire *in vitro* translation reactions were loaded onto 10-40 % (w/v) sucrose gradients (20 mM Tris pH 8, 20 mM $MgCl_2$, 100 mM $NH_4(OAc)$, 2 mM β-mercaptoethanol) and centrifuged 2 h at 40 000 rpm, 4 °C in SW41 rotor (Beckman Coulter). Polysomes profiles were obtained using Biocomp Piston Gradient Fractionator (BioComp Instruments) by measuring absorbance at 254 nm and 400 µl fractions were collected in 96 wells plates (Thermo Scientific).
Fractions collected from the polysomes profiles were precipitated with phenol/chloroform. One volume of phenol/chloroform/isoamyl alcohol was added to each fraction and samples were centrifuged at 15 000 rpm for 5 minutes at 4 °C. The aqueous upper phase was carefully collected. Sodium acetate 3M (1/10 of sample

volume), pure ethanol (2,5 volume) and Glycogen were added to the collected phase and samples were incubated overnight at -80 °C. Samples were centrifuged at 15 000 rpm for 30 minutes at 4 °C and the supernatants were then discarded. Pellets were washed with 200 µl of ethanol 70% (v/v) and centrifuged again at 15 000 rpm for 15 minutes at 4 °C. Pellets were set to dry on the bench before being resuspended in 20 µl of The RNA Storage Solution (Ambion, Thermo Fisher Scientific) and stored at -80 °C.

Northern Blotting – Precipitated RNAs (5 µl) or RNAsnap extracts were loaded on a 1% (w/v) agarose gel and then transferred to an Amersham Hybond-N+ membrane (Cytiva). After migration, 16S and 23S RNA were visualized with Ethidium Bromide (EtBr) under UV. RNAs were cross-linked on the membrane by exposing the membrane to UV for 30 s at 100 x 1 200 µJ / cm^2. The radioactive probe was prepared from 40 pmoles of D072 primer (**Table 1**) and labeled at the 5' end with 10 units of T4 polynucleotide kinase (New England Biolabs) and [γ-^{32}P]-ATP (150 µCi). After pre-incubation for 1 hour at 42 °C in the hybridization buffer (ULTRAhyb, Invitrogen Thermo Fisher Scientific), membranes were incubated with the probe, in the hybridization buffer, overnight at 42 °C. Membranes were washed three times (once in 2x SSC + 0.1% (v/v) SDS, once in 1x SSC + 0.1% (v/v) SDS and finally in 0.1x SSC + 0.1% (v/v) SDS) at 42 °C during 10 min. Radioactive signal was detected on a Typhoon 9 500 FLA scanner (GE Healthcare). Quantification of the EtBr and radioactive signals was performed with Fiji software (80). For the mRNA quantification experiments a loading control was done by rehybridizing the membrane with the 23S rRNA probe (C045, **table 1**).

Filter assay – To test the binding affinity of the TBT and TBT_G mRNA to the 30S ribosomal subunit we used PURExpress ΔRibosome Kit (NEB) supplemented with 5 µM of 30S ribosomal subunit and 10 µM $tRNA^{fMet}$ in the presence of 1.4 µM of radioactively labelled mRNA (prepared as described above by *in vitro* translation followed by [^{32}P] labelling as described for the northern blot probe labelling). 30S ribosome subunit were purified from *E. coli* strain MRE600 (79). The reaction was performed at 4 °C in the buffer: 20 mM Tris-HCl pH 7; 15 mM MgOAc; 100 mM NH_4OAc; 1 mM DTT. At 30, 60 and 300 sec, 4 µl of the reaction were taken and

deposited on a nitrocellulose filter (MF-Millipore 0.025 µm MCE Membrane) right after 2x 6 ml of reaction buffer was used to wash the filter under vacuum. Radioactive signal was detected on a Typhoon 9500 FLA scanner (GE Healthcare) and quantification of the signals was performed with Fiji software (80).

Computational modeling – In Figure 2, we observe that after transcription is blocked, some portion of the mRNA decays within the first minute and the remaining mRNA decays exponentially with a measurable rate Γ:

$$m(t) = F_0\delta_{t=0} + S_0 exp\{-\Gamma t\},$$

We will now describe how we arrive at this functional form with our proposed fast and slow population model of Figure 3C,

$$dF/dt = A - \beta F + \lambda S - \gamma F, \qquad dS/dt = \beta F - \lambda S.$$

The steady-state values for the Fast and Slow populations are

$$F_0 = A/\gamma, \qquad S_0 = \beta F_0/\lambda.$$

Blocking transcription sends $A \to 0$. The mRNA shows a bi-phasic decay, one with a decay time much less than 1 min and the other on the order of few minutes. To match the model, if we take $\gamma \gg 1$/min, we obtain the very rapid decay of the F population, approximating the delta-function above. Finally, we find that

$$S = S_0\, exp\{-\lambda t\},$$

solves the slow pool differential equation.

By fitting an exponential decay to the $t = 1,2,3,4$ minute time points, we obtain the slow fraction S_0 and rate parameter λ, which is related to half-life of the slow pool

$$\lambda = ln(2)/T_{HL}.$$

The fast fraction $F_0 = m_0 - S_0$, and the rate parameter $\beta = \lambda\, S_0/F_0$.

Estimation of the mRNA decay rate and half-life – The mRNA decay rate and half-life were estimated through the analysis of the decay data, as described in Figure 2 and Supplementary Figure 4. Using the *R* statistics program (81) the data were fitted to a single decay exponential model, represented by the equation, $S = S_0\, exp\{-\lambda t\}$. The plotting of the data was done using Prism 8 (GraphPad).

Statistics and Reproducibility – Statistical details can be found in the figure legends. Data were plotted using Prism 8 (GraphPad) and correlation were determined using

linear regression and the goodness of the fit r^2 were reported in the figures. All the experiments presented have been reproduced at least twice with the same results.

Results

A richness in the first codons increases protein expression. As it was shown in our previous global study performed in *E. coli (13),* the base composition of the first 18 nucleotides (6 codons) of the coding sequence, which comprise the area covered by the 70S initiation complex, has a strong impact on protein expression. Increase in A and decrease in G in this region show statistical correlation with protein expression. We decided to use the Venus YFP, as it is one of the most versatile and brightest fluorescent proteins (82) to investigate the role of this region in protein expression. First, we changed the 6 codons after the ATG of the YFP to synonymous ones, by either choosing ones with higher AT content for the YFP_A construction or by using the best synonymous codons according to our previously published codon metric (13) for YFP_M construction (**Figure 1A**). Secondly, we searched in *E. coli* genome for a highly-expressed gene (based on proteomic measurement) that is enriched in A in its first 7 codons and selected the enolase gene. We fused its first 21 nucleotides (which we call a "Translation Boosting Tag" (TBT)) to our YFP reporter (**Figure 1A**). Then, starting from the TBT-YFP construct (TBT), we took the reverse methodology *i.e*. replacing TBT codons by their synonymous codons containing the highest G fraction (TBT_G). To maintain near-physiological conditions, we utilized a low-copy plasmid (pMMB67EH plasmid (72)) expressing the YFP gene under the control of an IPTG-inducible pTac promoter, allowing expression by the native *E. coli* RNA polymerase.

The protein production of these YFP variants was first determined by measuring the fluorescence of colonies on agar plate (**Figure 1A, right**). From this result, we can see that all the constructs expressed more than the original YFP, and that the TBT construct expresses the most. Then to have a more quantitative and dynamic measurement of the expression, we measured the fluorescence during *E. coli* growth in liquid culture after IPTG induction at the start of the culture (**Figure 1B**). The lag in the fluorescence signal is due to the time necessary to have enough YFP expression to generate a fluorescence signal above the background and to the maturation time of the YFP Venus, which is 17.6 minutes (82). We estimated the protein synthesis rate (defined later one as *dP*/*dt,* in the mathematical model) by measuring the increase per

minute of the fluorescence normalized to the OD_{600} in the early linear part of the expression (**Supplementary Figure S2A**). This measurement will also include the refolding time for the YFP but since that should be similar for all constructs we did not correct for it. The protein synthesis rate varies widely across the constructs: 3.6 min^{-1} for YFP, 14.9 min^{-1} for YFP_M, 34.6 min^{-1} for YFP_A, 29.9 min^{-1} for TBT_G and 73.3 min^{-1} for TBT (**Figure 1B and C and Supplementary Figure S2A**). These results confirm that the A abundance is an important feature of the mRNA for its translation and that in this region, codons rich in A perform better that the best codons of the metric we published previously (13). The limit imposed by using only synonymous mutations can be surpassed by adding the TBT sequence. The TBT variant exhibits the highest expression among all YFP constructs (**Figure 1C and Supplementary Figure S2A**). However, the synonymous codon replacement with an increase in G content in the TBT_G construct significantly reduces expression to a similar level of the YFP_A construct. These findings highlight that incorporating the first six codons from a highly expressed *E. coli* gene can enhance the expression productivity of a poorly expressing gene with a low (A minus G) value. Furthermore, the results demonstrate a fourfold reduction in expression for the TBT constructs when A is decreased and G is increased.

Influence of N-terminal amino acids on protein expression. After 10 hours of growth, the TBT construct expressed protein at a level close to 3 times higher than the YFP_A construct (**Figure 1A and B**). While YFP_A has slightly more A in the first six codons than TBT (11 *vs.* 10), it also has much more G (7 *vs.* 2). Therefore, the lower protein expression from the YFP_A construct could be caused by its increased G content in this region. However, the two constructs also have different amino acid (aa) sequences, which could potentially directly influence their protein expression properties. The presence of positively charged amino acids at the beginning of the coding sequence has been shown to facilitate formation of the nascent peptide in bacteria (70) and yeast (12). In *Bacillus subtilis*, a Lys is found at position 2 in 20% of the genes (83). Moreover, the presence of a Lys codon in third position has been correlated with increased protein expression in *E. coli* (70). Given that the TBT construct has Lys residues at both positions 3 and 6, while the YFP_A construct has just a single Lys residue at position 4 (**Figure 1A**), the substantially higher expression of

the TBT construct could be influenced by the differences in its N-terminal aa sequence in addition to or instead of the differences in its nucleotide base composition in this region. It is fundamentally difficult to separate the influence of these two chemical features on translation efficiency given the inability to change the amino acid at a specific position in a protein sequence without changing the nucleotides encoding it. Therefore, to try to gain insight into their relative influence on the expression of the TBT *vs.* YFP_A constructs, we conducted a series of experiments comparing the effects of changing aa identity or interchanging aa positions in the first six codons.

We first substituted the GAG codon for Glu with the the AAA codon for Lys just at position 6 or at both positions 6 and 7 in YFP (**Supplementary Figures S2A and S3A-B**). The single-mutant YFP_{E6K} construct and the double-mutant YFP_{E6-7K} construct showed very similar ~2.3-fold increases in protein synthesis rate (8.4 and 8.3 min^{-1}, respectively) compared to YFP (3.6 min^{-1}). The modest gain in expression efficiency in the single-mutant YFP_{E6K} construct could be attributable either to the substitution of Lys for Glu or the substitution of two As for two Gs in the sixth codon or potentially influenced by both factors. The failure of exactly the same substitutions at the seventh codon to change expression level supports previous reports that the influence of A enrichment on protein expression is limited to the first 6 codons (13,17). To test the influence of having a Lys residue specifically at position 3 in the coding sequence, we swapped the Ser codon at position 3 and the Lys codon at position 4 in YFP to change the aa sequence at the N-terminus of the protein without altering the nucleotide base composition in this region (**Supplementary Figures S2A and S3A-B**). The protein synthesis rate of the resulting YFP_{StoK} construct was ~2.1-fold lower than the parental YFP construct (1.7 *vs.* 3.6 min^{-1}), showing that, at least in the context of the N-terminal aa sequence in YFP, having a lysine at position 3 does not increase protein expression when the nucleotide base content in this region remains constant.

To further evaluate the role of Lys residues at the first six positions in the coding sequence, we made the same pair of codon and aa substitutions (GAA for Glu or TTA for Leu) at each of the two Lys residues in this region of the TBT sequence, which are located at positions 3 and 6 and both encoded by the AAA codon (**Supplementary Figure S2A and S4A-B**). The Lys-to-Glu substitutions at both sites produce similar 21-32% reductions in protein synthesis rate (51.4 min^{-1} for TBT_{K3E} and 59.5 min^{-1} for TBT_{K6E} *vs.* 75.3 min^{-1} for TBT), which goes in the same direction but is smaller in

magnitude than the ~57% reduction observed when substituting the GAG codon for Glu for the AAA codon for Lys at position 6 in YFP (**Supplementary Figures S2A and S3A-B**). These observations reinforce the conclusion that Lys at position 3 does not have a unique influence on protein expression level compared to Lys at other positions in the first six codons. The very modest effect of the Lys-to-Glu substitutions in TBT could again be influenced by the change in aa identity in addition to or instead of the change in nucleotide base composition. Nonetheless, our results tend to weigh against the aa substitution being responsible for the effect because stereochemical interactions with the peptidyltransferase center and nascent-peptide exit tunnel, which presumably mediate aa effects, would be expected to be dependent on sequence position and context, while the effects of Lys-to-Glu substitution on protein expression observed in our experiments are not.

In contrast to the very similar impact of the substitutions in the TBT_{K3E} and TBT_{K6E} constructs, the substitutions in the TBT_{K3L} and TBT_{K6L} constructs have significantly different effects on protein expression depending on the site (**Supplementary Figure S2A and S4A-B**). Substituting the TTA codon for Leu for the AAA codon for Lys at position 6 in TBT produces an ~30% reduction in protein synthesis rate (53.0 min^{-1} for TBT_{K6L} *vs.* 75.3 min^{-1} for TBT), a very similar reduction to that observed when the GAA codon for Glu is introduced at either that position in the TBT_{K3E} construct or at position 6 in the TBT_{K6E} construct. A substantially larger ~74% reduction in protein synthesis rate is observed when the same substitution of the TTA codon for Leu for the AAA codon for Lys is made at position 3 in TBT (19.3 min^{-1} for TBT_{K3L} *vs.* 75.3 min^{-1} for TBT). Notably, protein expression from the TBT_{K3L} construct is somewhat lower than that from the TBT_{G} construct even though the former has 8 As and only 2 Gs in its first six codons *versus* 7 As and 6 Gs in the latter. The strong position/context-dependence of the Lys-to-Leu substitutions in TBT, as well as that of the codon swap in the YFP_{StoK} construct reported above, suggests some specific stereochemical interactions contribute to the observed variations in protein expression efficiency, although these interactions could potentially involve either the first six amino acids in the nascent protein or the corresponding codons in the mRNA.

Importantly, in all of the aa/codon substitution experiments reported here, reducing A content in the first six codons consistently reduces protein expression to at least some extent. While our results do not rule out aa content in this region influencing protein

expression, they do not provide direct evidence for such an effect. In contrast, they provide extensive evidence that increasing A content or decreasing G content in the first six codons increases protein expression.

The A richness of the first codons improve in vitro protein expression. *In vitro* translation assays (IVTA) programmed with purified mRNA of the different constructs were conducted (**Figure 1D and Supplementary Figure S2B, S3C and S4C**) in minimal translation assay (PURE express from NEB). The fluorescence signal of the YFP was monitored and western blots of the final reaction revelated with anti-GFP antibody confirmed that the fluorescence signal correlates with the YFP amount (**Figure 1D**). Even if we can't directly link the *in vivo* and *in vitro* kinetics because the ratios of mRNA/ribosome are different, it is noticeable to see that the YFP has a similar protein synthesis rate in both conditions (3.6 min^{-1}) whereas TBT expression rate increases by more than 6 times *in vitro* (493.7 min^{-1} *in vitro* vs 73.3 min^{-1} *in vivo*) (**Supplementary Figure S2B**). Overall, all the constructs show a gain of expression when the frequency of A increases, this confirms that the observed effect of the first codons mostly influences mRNA translation *in vivo* and *in vitro*. Nevertheless, some constructs perform differently compared to *in vivo*. YFP_{StoK} is more expressed *in vitro* than the YFP with a rate of 9 min^{-1} vs 3.4 min^{-1}. On the other hand, TBT_G is less expressed *in vitro* than *in vivo*, making the difference with the TBT construct even more pronounced. The translation of these mRNAs is likely modulated by factors that are present *in vivo* but not in the IVTA which is composed of the minimal set of translation factors and ribosomes (84).

Steady state mRNA levels of each construct correlate with their protein expression level. We determined the mRNA levels in a steady state for various YFP constructs through northern blot analysis at different time points after induction with IPTG (0, 10, 60, and 120 minutes) (**Figure 2 and Supplementary Figure S3D**). The northern blot utilizes a DNA probe that hybridizes with the 3'UTR of the mRNA. The TBT construct exhibits the highest mRNA concentration, while YFP has the lowest as they do for protein production. Overall, for all constructs, the mRNA concentration correlates with the produced protein levels. The same trend is observed for the YFP and TBT amino acid variants (**Supplementary Figure S3D and S4D).** Given that all

constructions were expressed using the same pTac promoter, we hypothesize that the variation in mRNA levels is caused by RNA degradation rather than transcription. To assess mRNA stability, we inhibited transcription with rifampicin after 10 minutes of induction by IPTG and determined by northern blot the mRNA concentration at 1-minute intervals (**Figure 2**).

After just 1 minute of transcription inhibition, the full-length messenger RNA for the YFP and YFP_M constructs was undetectable, but for YFP_A and the two TBT constructs a population of more stable mRNA was detectable. The signals before and after rifampicin treatment clearly suggests two populations: one with a fast decay (much less that 1 min) and for some constructs (YFP_A and the two TBT), a second one with a slower rate for which we can calculate the half-life (1.25 min for YFP_A, 0.9 min for TBT_G and 3.41 min for TBT). The signal was quantified and normalized relative to the YFP construct's mRNA concentration before rifampicin treatment. For the constructs showing a slow decay population the fraction of the fast decay population (F_0) was extrapolated by fitting the slow decay to an exponential decay and taking the intercept with the y axis as the proportion of slow decay (S_0); the F_0 being the difference between the steady-state mRNA concentration and the S_0 fraction. The YFP aa variants (**Supplementary Figure S3D**) also show only a fast decay, but the TBT aa variants show the two decay rates (**Supplementary Figure S4D**).

Translation by the ribosome is the major determinant of mRNA stability. We looked for correlations between the experimentally determined rates and populations. First, we looked at correlation between the protein expression determined by the YFP fluorescence *in vivo* and the fast and slow mRNA populations, F_0 and S_0 (**Figure 3A**). F_0 is not correlated with fluorescence, suggesting that the F_0 population of mRNA is not translated by the ribosome. On the other hand, the S_0 decay shows a clear correlation with protein expression rate (r^2=0.82) suggesting that this population of mRNA is the productive one. Secondly, correlation between the expression *in vivo* as monitored by the fluorescence intensity and the steady state mRNA concentration (10 min after induction) shows a linear correlation between the two variables (**Figure 3B**) confirming that the amount of mRNA and translation are linked. Unexpectedly, *in vitro* expression of the constructs in the IVTA with a fixed concentration of each mRNA (1.4 μM) also correlates with the *in vivo* steady state mRNA (**Figure 3B**). Since the only

common parameter is the translation of the mRNA by the ribosome, it clearly demonstrates that the decay is dependent on the translation efficiency.

Mathematical model that explains the two-mRNA decay rates. In a standard "Central Dogma" model (**Figure 3C**), mRNA (m) is transcribed and degraded, and used as a template for protein production (dP/dt), which yields a simple dynamical model:

$$(1) \quad dm/dt = A - \gamma m,\ dP/dt = \rho m,$$

with transcription rate A, mRNA degradation rate γ, and translation rate ρ. In steady state,

$$(2) \quad m_0 = A/\gamma,\ dP/dt = \rho m_0.$$

This simple model predicts that the *in vivo* protein production rate increases proportional to the steady-state mRNA level; however, we notably observe in **Figure 3B** that the protein production rate goes to zero at a finite mRNA amount,

$$(3) \quad dP/dt = \rho(m - m_{min}),$$

while the simple model has no such m_{min} offset.

In the decay experiments, when rifampicin shuts off mRNA transcription, $A \to 0$. The standard Central Dogma model solution predicts a simple exponential mRNA decay $m(t) = m_0 exp(-\gamma t)$. However, the experiments instead show a biphasic decay, with a fast portion F_0 decaying within the first minute, and a slow portion S_0 decaying with half-lives ranging from 1 to 4 minutes (**Figure 2, 3A and Supplementary Figure S4D**). To mathematically describe the biphasic decay, we propose a new model that contains two categories of mRNA, $m = F + S$, with Fast F and Slow S decaying populations,

$$(4) \quad dF/dt = A - \beta F + \lambda S - \gamma F,\ dS/dt = \beta F - \lambda S.$$

The parameters β and λ are the rates of conversion between the Fast and Slow populations (**Figure 3C**). We propose that β is the 70S ribosome initiation complex formation rate, which is sensitive to the mRNA folding at the beginning of the coding sequence. The steady-state values are:

$$(5) \quad F_0 = A/\gamma,\ S_0 = \beta F_0/\lambda.$$

Note that the Fast proportion F_0 is determined by the transcription rate A and fast degradation rate γ, so F_0 is predicted not to depend on the ribosome-binding rate, which

is consistent with **Figure 3A**. However, the Slow component's proportion S_0 increases with ribosome binding rate β and thus with initiation rate.

After rifampicin treatment, $A \to 0$, and given a rapid decay rate $\gamma \gg 1/\text{min}$, we assume the fast portion F_0 has essentially disappeared by the 1 min time point (captured with the delta-function below). This allows us to fit the **Figure 3C** decay data to

$$(6) \quad m(t) = F_0\delta_{t=0} + S_0 exp(-\Gamma t),$$

which is essentially a single exponential decay to the $t = 1,2,3,4$ minute time points in that experiment. Extrapolating to $t = 0$ thus gives S_0 and F_0.

Among the various construct sequences, we see that the *in vivo* protein production rate is proportional to S_0, but is independent of F_0, as shown in **Figure 3A**. This finding is consistent with our interpretation that β is the 70S ribosome formation rate. Statistical physics suggests β is proportional to the Boltzmann likelihood of the ribosome binding site on the mRNA being single-stranded,

$$(7) \quad \beta \sim p_{single} \sim exp(\Delta G/kT^*).$$

Using BindOligoNet model(85), we predict the free energy cost

$$(8) \quad \Delta G = 1 - 0.1N_A + 0.4N_C + 1.0N_G + 0.1N_T$$

(in kcal/mol) to unfold a region of mRNA. Increasing the number of adenosines N_A and decreasing the number of guanosines N_G has the strongest effect on the initiation rate and protein production. Indeed, we find a Pearson correlation of R=0.88 between ΔG and the logarithm of the protein-production rate, as predicted in the Boltzmann formula above. In **Figure 3A**, we see that F_0 across the different constructs is uncorrelated with protein expression, consistent with the steady-state formulas above. We also find $F_o \approx m_{min}$.

Increase of A in the first codon promotes the formation of the 70S IC complex.

In order to understand the molecular mechanism that leads to the expression defect, we compared the TBT and TBT_G mRNA abilities to bind the 30S ribosomal subunit using a filter binding assay. The assay demonstrated that the two constructs bind to the 30S subunit with the same affinity (**Figure 4A**). Therefore, the A content in the first codons seems to not affect the interaction between the 30S subunit and the mRNA.

However, it is possible that the mRNA is not correctly positioning itself within the mRNA channel of the 30S ribosomal subunit.

To gain an overview of the differences during the translation of the two mRNAs, we conducted an IVTA with each mRNA. After 1-hour of reaction, we separated each reaction on sucrose gradient, collected the fractions, and extracted the total RNA (**Figure 4B**). We first tried to use the fluorescence of the MGapt aptamer (77,86) that we added in the 3'UTR of our transcript, but the fluorescence signal was too low for detection (data not shown). Therefore, we determined, through northern blot analysis, the location of the mRNA within each profile. Several observations emerged from this experiment. First, the TBT_G mRNA produced fewer polysomes, and consequently, less mRNA was found in the polysome fractions (**Figure 4C**), suggesting a reduced entry of ribosomes into the elongation cycle. Secondly, depletion of TBT_G mRNA in the polysome led to an accumulation in the 30S-50S fractions (**Figure 4C and 4D**). This accumulation correlates with an increase in 16S rRNA in the 50S fraction, indicating a trailing of the pre-30S initiation complex within the 50S location. From these observations we conclude that the constructs have a similar affinity for the 30S ribosomal subunit and that the TBT_G variant affects the formation of the 70S Initiation Complex (IC) after formation of the 30S pre-IC or the 30S IC.

The TBT sequence can be used to increase protein production. To assess whether the TBT sequence can enhance the expression of proteins other than YFP, we fused it to the 5'-end of genes encoding proteins with poor expression levels. Genes *ycaQ* (*E. coli*), RSP_2139 (*Rhodobacter sphaeroides*), SCO1897 (*Streptomyces coelicolor*) and SRU_1983 (*Salinibacter ruber*) were previously assessed for their expression in the *E. coli* Bl21 DE3 strain (13). This evaluation was conducted utilizing a pET21 plasmid, placing the expression of the gene under the control of a T7 promoter. The WT constructs exhibited negligible to very low expression levels (13) (**Figure 5A**). Upon introducing the TBT tag fused to the N-terminus of the protein, we observed a significant improvement in the expression of *ycaQ*, SRU_1983 and RSP_2139, as well as an observable gain in the expression of SCO1897 (**Figure 5A**). These findings underscore the significance of the first codons in achieving higher protein expression and highlight the TBT tag as an accessible and cost-effective option for boosting the expression of certain proteins. They also demonstrate that the A

richness effect of the early codons is not dependent on the native polymerase of *E. coli* and can be observed when genes are transcribed with a phage T7 polymerase, which uncouples transcription from translation (5,87).

Discussion

In this study, we present results supporting a model (**Figure 5B**) in which the base composition of the first six codons controls both the translation efficiency and stability of mRNAs in *E. coli*. This effect is mediated by the formation of the 70S IC, which is promoted by early codons enriched in A and depleted in G. The A richness of the mRNA does not seem to affect its binding affinity for the 30S subunit, but it does influence the formation of the 70S IC. Free mRNAs and those bound to the 30S but not matured into the mRNA 70S IC complex are non-productive, forming a population of rapidly decaying mRNA. This model implies that successful initiation of translation by the ribosome is a major factor dictating mRNA stability, a proposal that aligns with the established understanding of this step as a pivotal checkpoint in mRNA selection (88).

We built a mathematical model (**Figure 3C**), that describes the biphasic mRNA decay observed in our experiments (**Figure 2** and **Supplementary Figure S4D**) by postulating two populations. Protein production level is proportional to the slowly decaying mRNA population, while the fast-decaying mRNA population is uncorrelated with protein level (**Figure 3A**). Our model differs from the usual "translation efficiency" assumption (Eq 1) of proportionality between protein rate and total mRNA, instead invoking a substantial population of unproductive mRNA (Eq 3). A Boltzmann factor with an unfolding free energy given by Eqs 7-8 predicts the ribosome initiation rate (**Figure 3D**), explaining why A-rich and G-poor sequences are translated at higher rates. Our model predicts that the initiating ribosome is the pivot that switches the fast-decaying mRNA population toward the slow-decaying population.

This model of mRNA degradation should drive directional decay of the mRNA from the 5' to the 3', despite the absence of a 5' to 3' processive RNase in *E. coli*. The polarity, as previously described in the literature (89,90), may arise from the accessibility and phosphorylation state of the 5’-end of the mRNA for the main *E. coli* Rnase, Rnase E (91-93). The polarity of decay is then controlled by the scanning ability of the RNase E

(94). This model aligns with the ribosomal mRNA protection model (94), but it suggests that interaction with the 30S subunit alone does not provide protection against mRNA degradation but instead controls a competition between degradation and translation initiation. Future research should aim to characterize the molecular conformation and interactions of the abortive 30S IC and how it funnels mRNA to degradation enzymes.

In conclusion, we propose that the ribosome-docking region in an mRNA and specifically the first six encoding codons play a pivotal role in orchestrating a dynamic competition between mRNA decay and translation initiation. Initiation of mRNA decay primarily upstream (5') of translating ribosomes is a mechanism that reconciles disparate observations (13,15,17,21,56,69,70,95). This paradigm optimizes metabolic efficiency, by ensuring that mRNA decay is initiated upstream of translating ribosomes rather than downstream. This regulatory mechanism will prevent the wasteful expenditure of energy involved in the production and subsequent degradation of partially synthesized proteins.

The research reported in this paper also establishes a cost-efficient and straightforward strategy to enhance protein expression in *E. coli* by fusing target proteins after the Translation-Boosting Tag (TBT) sequence. We showed that this tag can boost the expression of proteins transcribed either by the native *E. coli* RNA polymerase or by the phage T7 polymerase. This tag also enhances protein expression in cell-free *in vitro* translation systems.

Data availability

The data underlying this article are available in the article and in its online supplementary material.

Acknowledgement

We thank Farès Ousalem for sharing some of his purified 70S ribosomes.

Funding

AL, LM, SN, TO and GB were supported by funds from the CNRS (UMR8261), Université Paris Cité, the LABEX program (DYNAMO ANR-11-LABX-0011) and two ANR grants (EZOtrad/ANR-14-ACHN-0027 and ABC-F_AB/ANR-18-CE35-0010).

Author contributions

AL and LM with the help of SN, TO and CB performed the experiments. AL, LM and GB analyzed the data. IW, JFH, DPA and GB built the mathematical model. AL, LM and GB prepared the figures. GB designed the research program. AL, LM, DPA, JFH and GB wrote the manuscript in consultation with the other authors.

Conflict of interest

The authors declare no competing financial interests.

References

1. Chaney, J.L. and Clark, P.L. (2015) Roles for Synonymous Codon Usage in Protein Biogenesis. *Annu Rev Biophys*, **44**, 143-166.
2. Hunt, R.C., Simhadri, V.L., Iandoli, M., Sauna, Z.E. and Kimchi-Sarfaty, C. (2014) Exposing synonymous mutations. *Trends Genet*.
3. Zhang, F., Saha, S., Shabalina, S.A. and Kashina, A. (2010) Differential arginylation of actin isoforms is regulated by coding sequence-dependent degradation. *Science*, **329**, 1534-1537.
4. Chen, G.T. and Inouye, M. (1994) Role of the AGA/AGG codons, the rarest codons in global gene expression in Escherichia coli. *Genes & development*, **8**, 2641-2652.
5. Chevrier-Miller, M., Jacques, N., Raibaud, O. and Dreyfus, M. (1990) Transcription of single-copy hybrid lacZ genes by T7 RNA polymerase in Escherichia coli: mRNA synthesis and degradation can be uncoupled from translation. *Nucleic acids research*, **18**, 5787-5792.
6. Dong, H., Nilsson, L. and Kurland, C.G. (1996) Co-variation of tRNA abundance and codon usage in Escherichia coli at different growth rates. *J Mol Biol*, **260**, 649-663.
7. Chen, G.F. and Inouye, M. (1990) Suppression of the negative effect of minor arginine codons on gene expression; preferential usage of minor codons within the first 25 codons of the Escherichia coli genes. *Nucleic acids research*, **18**, 1465-1473.
8. Goldman, E., Rosenberg, A.H., Zubay, G. and Studier, F.W. (1995) Consecutive low-usage leucine codons block translation only when near the 5' end of a message in Escherichia coli. *J Mol Biol*, **245**, 467-473.

9. Caskey, C.T., Beaudet, A. and Nirenberg, M. (1968) RNA codons and protein synthesis. 15. Dissimilar responses of mammalian and bacterial transfer RNA fractions to messenger RNA codons. *J Mol Biol*, **37**, 99-118.

10. Ikemura, T. (1981) Correlation between the abundance of Escherichia coli transfer RNAs and the occurrence of the respective codons in its protein genes: a proposal for a synonymous codon choice that is optimal for the E. coli translational system. *J Mol Biol*, **151**, 389-409.

11. Goodman, D.B., Church, G.M. and Kosuri, S. (2013) Causes and Effects of N-Terminal Codon Bias in Bacterial Genes. *Science*, **342**, 475-479.

12. Dao Duc, K. and Song, Y.S. (2018) The impact of ribosomal interference, codon usage, and exit tunnel interactions on translation elongation rate variation. *PLOS Genetics*, **14**, e1007166.

13. Boël, G., Letso, R., Neely, H., Price, W.N., Wong, K.-H., Su, M., Luff, J.D., Valecha, M., Everett, J.K., Acton, T.B. *et al.* (2016) Codon influence on protein expression in E. coli correlates with mRNA levels. *Nature*, **529**, 358-363.

14. Elf, J., Nilsson, D., Tenson, T. and Ehrenberg, M. (2003) Selective charging of tRNA isoacceptors explains patterns of codon usage. *Science*, **300**, 1718-1722.

15. Li, G.W., Oh, E. and Weissman, J.S. (2012) The anti-Shine-Dalgarno sequence drives translational pausing and codon choice in bacteria. *Nature*, **484**, 538-541.

16. Li, G.W., Burkhardt, D., Gross, C. and Weissman, J.S. (2014) Quantifying absolute protein synthesis rates reveals principles underlying allocation of cellular resources. *Cell*, **157**, 624-635.

17. Bentele, K., Saffert, P., Rauscher, R., Ignatova, Z. and Blüthgen, N. (2013) Efficient translation initiation dictates codon usage at gene start. *Molecular systems biology*, **9**, 675.

18. Novoa, E.M. and Ribas de Pouplana, L. (2012) Speeding with control: codon usage, tRNAs, and ribosomes. *Trends Genet*, **28**, 574-581.

19. Komar, A.A. (2016) The Yin and Yang of codon usage. *Human molecular genetics*, **25**, R77-R85.

20. Kåhrström, C.T. (2012) Bacterial physiology: Setting the speed of translation. *Nat Rev Micro*, **10**, 375-375.

21. Kudla, G., Murray, A.W., Tollervey, D. and Plotkin, J.B. (2009) Coding-Sequence Determinants of Gene Expression in Escherichia coli. *Science*, **324**, 255-258.

22. Pop, C., Rouskin, S., Ingolia, N.T., Han, L., Phizicky, E.M., Weissman, J.S. and Koller, D. (2014) Causal signals between codon bias, mRNA structure, and the efficiency of translation and elongation. *Molecular systems biology*, **10**, 770.

23. Ingolia, N.T., Ghaemmaghami, S., Newman, J.R. and Weissman, J.S. (2009) Genome-wide analysis in vivo of translation with nucleotide resolution using ribosome profiling. *Science*, **324**, 218-223.

24. Quax, T.E., Wolf, Y.I., Koehorst, J.J., Wurtzel, O., van der Oost, R., Ran, W., Blombach, F., Makarova, K.S., Brouns, S.J., Forster, A.C. *et al.* (2013)

Differential translation tunes uneven production of operon-encoded proteins. *Cell reports*, **4**, 938-944.

25. Mohammad, F., Woolstenhulme, C.J., Green, R. and Buskirk, A.R. (2016) Clarifying the Translational Pausing Landscape in Bacteria by Ribosome Profiling. *Cell reports*, **14**, 686-694.

26. Woolstenhulme, C.J., Guydosh, N.R., Green, R. and Buskirk, A.R. (2015) High-precision analysis of translational pausing by ribosome profiling in bacteria lacking EFP. *Cell reports*, **11**, 13-21.

27. Hussmann, J.A., Patchett, S., Johnson, A., Sawyer, S. and Press, W.H. (2015) Understanding Biases in Ribosome Profiling Experiments Reveals Signatures of Translation Dynamics in Yeast. *PLoS genetics*, **11**, e1005732.

28. Hussmann, J.A. and Press, W.H. (2014) Local correlations in codon preferences do not support a model of tRNA recycling. *Cell reports*, **8**, 1624-1629.

29. Gritsenko, A.A., Hulsman, M., Reinders, M.J. and de Ridder, D. (2015) Unbiased Quantitative Models of Protein Translation Derived from Ribosome Profiling Data. *PLoS Comput Biol*, **11**, e1004336.

30. Zamora-Romo, E., Cruz-Vera, L.R., Vivanco-Dominguez, S., Magos-Castro, M.A. and Guarneros, G. (2007) Efficient expression of gene variants that harbour AGA codons next to the initiation codon. *Nucleic acids research*, **35**, 5966-5974.

31. Chevance, F.F.V. and Hughes, K.T. (2017) Case for the genetic code as a triplet of triplets. *Proceedings of the National Academy of Sciences of the United States of America*, **114**, 4745-4750.

32. Chevance, F.F., Le Guyon, S. and Hughes, K.T. (2014) The effects of codon context on in vivo translation speed. *PLoS genetics*, **10**, e1004392.

33. Höllerer, S. and Jeschek, M. (2023) Ultradeep characterisation of translational sequence determinants refutes rare-codon hypothesis and unveils quadruplet base pairing of initiator tRNA and transcript. *Nucleic acids research*, **51**, 2377-2396.

34. Mustoe, A.M., Busan, S., Rice, G.M., Hajdin, C.E., Peterson, B.K., Ruda, V.M., Kubica, N., Nutiu, R., Baryza, J.L. and Weeks, K.M. (2018) Pervasive Regulatory Functions of mRNA Structure Revealed by High-Resolution SHAPE Probing. *Cell*, **173**, 181-195.e118.

35. Dana, A. and Tuller, T. (2014) The effect of tRNA levels on decoding times of mRNA codons. *Nucleic acids research*, **42**, 9171-9181.

36. dos Reis, M. (2003) Unexpected correlations between gene expression and codon usage bias from microarray data for the whole Escherichia coli K-12 genome. *Nucleic acids research*, **31**, 6976-6985.

37. Pelechano, V., Wei, W. and Steinmetz, Lars M. (2015) Widespread Co-translational RNA Decay Reveals Ribosome Dynamics. *Cell*, **161**, 1400-1412.

38. Presnyak, V., Alhusaini, N., Chen, Y.H., Martin, S., Morris, N., Kline, N., Olson, S., Weinberg, D., Baker, K.E., Graveley, B.R. *et al.* (2015) Codon optimality is a major determinant of mRNA stability. *Cell*, **160**, 1111-1124.

39. Bazzini, A.A., Del Viso, F., Moreno-Mateos, M.A., Johnstone, T.G., Vejnar, C.E., Qin, Y., Yao, J., Khokha, M.K. and Giraldez, A.J. (2016) Codon identity regulates mRNA stability and translation efficiency during the maternal-to-zygotic transition. *The EMBO journal*, **35**, 2087-2103.

40. Mishima, Y. and Tomari, Y. (2016) Codon Usage and 3' UTR Length Determine Maternal mRNA Stability in Zebrafish. *Molecular cell*, **61**, 874-885.

41. Wu, Q., Medina, S.G., Kushawah, G., DeVore, M.L., Castellano, L.A., Hand, J.M., Wright, M. and Bazzini, A.A. (2019) Translation affects mRNA stability in a codon-dependent manner in human cells. *Elife*, **8**.

42. Mishima, Y., Han, P., Ishibashi, K., Kimura, S. and Iwasaki, S. (2022) Ribosome slowdown triggers codon-mediated mRNA decay independently of ribosome quality control. *The EMBO Journal*, **41**, e109256.

43. Saito, K., Kratzat, H., Campbell, A., Buschauer, R., Burroughs, A.M., Berninghausen, O., Aravind, L., Green, R., Beckmann, R. and Buskirk, A.R. (2022) Ribosome collisions induce mRNA cleavage and ribosome rescue in bacteria. *Nature*.

44. Grigoriadou, C., Marzi, S., Kirillov, S., Gualerzi, C.O. and Cooperman, B.S. (2007) A Quantitative Kinetic Scheme for 70 S Translation Initiation Complex Formation. *Journal of Molecular Biology*, **373**, 562-572.

45. Kaledhonkar, S., Fu, Z., Caban, K., Li, W., Chen, B., Sun, M., Gonzalez, R.L. and Frank, J. (2019) Late steps in bacterial translation initiation visualized using time-resolved cryo-EM. *Nature*, **570**, 400-404.

46. Godefroy-Colburn, T., Wolfe, A.D., Dondon, J., Grunberg-Manago, M., Dessen, P. and Pantaloni, D. (1975) Light-scattering studies showing the effect of initiation factors on the reversible dissociation of Escherichia coli ribosomes. *Journal of Molecular Biology*, **94**, 461-478.

47. Blumberg, B.M., Nakamoto, T. and Kézdy, F.J. (1979) Kinetics of initiation of bacterial protein synthesis. *Proceedings of the National Academy of Sciences of the United States of America*, **76**, 251-255.

48. Riba, A., Di Nanni, N., Mittal, N., Arhné, E., Schmidt, A. and Zavolan, M. (2019) Protein synthesis rates and ribosome occupancies reveal determinants of translation elongation rates. *Proceedings of the National Academy of Sciences*, **116**, 15023-15032.

49. Bremer, H. and Dennis, P.P. (2008) Modulation of Chemical Composition and Other Parameters of the Cell at Different Exponential Growth Rates. *EcoSal Plus*, **3**.

50. Metelev, M., Lundin, E., Volkov, I.L., Gynnå, A.H., Elf, J. and Johansson, M. (2022) Direct measurements of mRNA translation kinetics in living cells. *Nat Commun*, **13**, 1852.

51. Rodnina, M.V. (2018) Translation in Prokaryotes. *Cold Spring Harb Perspect Biol*, **10**.

52. Saito, K., Green, R. and Buskirk, A.R. (2020) Translational initiation in E. coli occurs at the correct sites genome-wide in the absence of mRNA-rRNA base-pairing. *eLife*, **9**, e55002.

53. Hersch, S.J., Elgamal, S., Katz, A., Ibba, M. and Navarre, W.W. (2014) Translation initiation rate determines the impact of ribosome stalling on bacterial protein synthesis. *J Biol Chem*, **289**, 28160-28171.

54. Ferrin, M.A. and Subramaniam, A.R. (2017) Kinetic modeling predicts a stimulatory role for ribosome collisions at elongation stall sites in bacteria. *eLife*, **6**, e23629.

55. Kosuri, S., Goodman, D.B., Cambray, G., Mutalik, V.K., Gao, Y., Arkin, A.P., Endy, D. and Church, G.M. (2013) Composability of regulatory sequences controlling transcription and translation in Escherichia coli. *Proceedings of the National Academy of Sciences*, **110**, 14024-14029.

56. Gu, W., Zhou, T. and Wilke, C.O. (2010) A Universal Trend of Reduced mRNA Stability near the Translation-Initiation Site in Prokaryotes and Eukaryotes. *PLoS Comput Biol*, **6**, e1000664.

57. Cambray, G., Guimaraes, J.C. and Arkin, A.P. (2018) Evaluation of 244,000 synthetic sequences reveals design principles to optimize translation in Escherichia coli. *Nature biotechnology*, **36**, 1005-1015.

58. Cetnar, D.P. and Salis, H.M. (2021) Systematic Quantification of Sequence and Structural Determinants Controlling mRNA stability in Bacterial Operons. *ACS Synthetic Biology*, **10**, 318-332.

59. Chiaruttini, C. and Guillier, M. (2020) On the role of mRNA secondary structure in bacterial translation. *WIREs RNA*, **11**, e1579.

60. Komarova, E.S., Chervontseva, Z.S., Osterman, I.A., Evfratov, S.A., Rubtsova, M.P., Zatsepin, T.S., Semashko, T.A., Kostryukova, E.S., Bogdanov, A.A., Gelfand, M.S. *et al.* (2020) Influence of the spacer region between the Shine-Dalgarno box and the start codon for fine-tuning of the translation efficiency in Escherichia coli: Influence of mRNA spacer on translation. *Microb. Biotechnol.*

61. Shultzaberger, R.K., Bucheimer, R.E., Rudd, K.E. and Schneider, T.D. (2001) Anatomy of Escherichia coli ribosome binding sites 1 1Edited by D. Draper. *Journal of Molecular Biology*, **313**, 215-228.

62. Osterman, I.A., Evfratov, S.A., Sergiev, P.V. and Dontsova, O.A. (2013) Comparison of mRNA features affecting translation initiation and reinitiation. *Nucleic acids research*, **41**, 474-486.

63. Reeve, B., Hargest, T., Gilbert, C. and Ellis, T. (2014) Predicting Translation Initiation Rates for Designing Synthetic Biology. *Front. Bioeng. Biotechnol.*, **2**.

64. Chen, H., Pomeroy-Cloney, L., Bjerknes, M., Tam, J. and Jay, E. (1994) The influence of adenine-rich motifs in the 3 prime portion of the ribosome binding site on human IFN-gamma gene expression in Escherichia coli. *J Mol Biol*, **240**, 20-27.

65. Lipońska, A., Ousalem, F., Aalberts, D.P., Hunt, J.F. and Boël, G. (2019) The new strategies to overcome challenges in protein production in bacteria. *Microbial biotechnology*, **12**, 44-47.

66. Hess, J.M., Jannen, W.K. and Aalberts, D.P. (2022) The Four mRNA Bases Have Quite Different (Un)folding Free Energies, Applications to RNA Splicing and Translation Initiation with BindOligoNet. *Journal of Molecular Biology*, 167578.

67. Cifuentes-Goches, J.C., Hernández-Ancheyta, L., Guarneros, G., Oviedo, N. and Hernández-Sánchez, J. (2019) Domains two and three of Escherichia coli ribosomal S1 protein confers 30S subunits a high affinity for downstream A/U-rich mRNAs. *The Journal of Biochemistry*, **166**, 29-40.

68. Duval, M., Korepanov, A., Fuchsbauer, O., Fechter, P., Haller, A., Fabbretti, A., Choulier, L., Micura, R., Klaholz, B.P., Romby, P. *et al.* (2013) Escherichia coli ribosomal protein S1 unfolds structured mRNAs onto the ribosome for active translation initiation. *PLoS biology*, **11**, e1001731.

69. Osterman, I.A., Chervontseva, Z.S., Evfratov, S.A., Sorokina, A.V., Rodin, V.A., Rubtsova, M.P., Komarova, E.S., Zatsepin, T.S., Kabilov, M.R., Bogdanov, A.A. *et al.* (2020) Translation at first sight: the influence of leading codons. *Nucleic acids research*, **48**, 6931-6942.

70. Verma, M., Choi, J., Cottrell, K.A., Lavagnino, Z., Thomas, E.N., Pavlovic-Djuranovic, S., Szczesny, P., Piston, D.W., Zaher, H.S., Puglisi, J.D. *et al.* (2019) A short translational ramp determines the efficiency of protein synthesis. *Nature communications*, **10**, 5774.

71. Meselson, M. and Yuan, R. (1968) DNA restriction enzyme from E. coli. *Nature*, **217**, 1110-1114.

72. Fürste, J.P., Pansegrau, W., Frank, R., Blöcker, H., Scholz, P., Bagdasarian, M. and Lanka, E. (1986) Molecular cloning of the plasmid RP4 primase region in a multi-host-range tacP expression vector. *Gene*, **48**, 119-131.

73. Blattner, F.R., Plunkett, G., Bloch, C.A., Perna, N.T., Burland, V., Riley, M., Collado-Vides, J., Glasner, J.D., Rode, C.K., Mayhew, G.F. *et al.* (1997) The Complete Genome Sequence of Escherichia coli K-12. *Science*, **277**, 1453-1462.

74. Studier, F.W. and Moffatt, B.A. (1986) Use of bacteriophage T7 RNA polymerase to direct selective high-level expression of cloned genes. *Journal of Molecular Biology*, **189**, 113-130.

75. Otsuka, Y., Muto, A., Takeuchi, R., Okada, C., Ishikawa, M., Nakamura, K., Yamamoto, N., Dose, H., Nakahigashi, K., Tanishima, S. *et al.* (2015) GenoBase: comprehensive resource database of Escherichia coli K-12. *Nucleic acids research*, **43**, D606-617.

76. Fostier, C.R., Ousalem, F., Leroy, E.C., Ngo, S., Soufari, H., Innis, C.A., Hashem, Y. and Boël, G. (2023) Regulation of the macrolide resistance ABC-F translation factor MsrD. *Nature Communications*, **14**, 3891.

77. Siegal-Gaskins, D., Tuza, Z.A., Kim, J., Noireaux, V. and Murray, R.M. (2014) Gene Circuit Performance Characterization and Resource Usage in a Cell-Free "Breadboard". *ACS Synthetic Biology*, **3**, 416-425.

78. Stead, M.B., Agrawal, A., Bowden, K.E., Nasir, R., Mohanty, B.K., Meagher, R.B. and Kushner, S.R. (2012) RNA snap ™: a rapid, quantitative and inexpensive, method for isolating total RNA from bacteria. *Nucleic acids research*, **40**, e156-e156.

79. Ousalem, F., Ngo, S., Oïffer, T., Omairi-Nasser, A., Hamon, M., Monlezun, L. and Boël, G. (2023) Global regulation via modulation of ribosome pausing by EttA. *bioRxiv*, 2023.2010.2017.562674.

80. Schindelin, J., Arganda-Carreras, I., Frise, E., Kaynig, V., Longair, M., Pietzsch, T., Preibisch, S., Rueden, C., Saalfeld, S., Schmid, B. *et al.* (2012) Fiji: an open-source platform for biological-image analysis. *Nature methods*, **9**, 676-682.

81. Team, R.C. (2012) R: A language and environment for statistical computing.

82. Nagai, T., Ibata, K., Park, E.S., Kubota, M., Mikoshiba, K. and Miyawaki, A. (2002) A variant of yellow fluorescent protein with fast and efficient maturation for cell-biological applications. *Nature biotechnology*, **20**, 87-90.

83. Leroy, M., Piton, J., Gilet, L., Pellegrini, O., Proux, C., Coppee, J.Y., Figaro, S. and Condon, C. (2017) Rae1/YacP, a new endoribonuclease involved in ribosome-dependent mRNA decay in Bacillus subtilis. *The EMBO journal*, **36**, 1167-1181.

84. Shimizu, Y., Inoue, A., Tomari, Y., Suzuki, T., Yokogawa, T., Nishikawa, K. and Ueda, T. (2001) Cell-free translation reconstituted with purified components. *Nature biotechnology*, **19**, 751-755.

85. Hess, J.M., Jannen, W.K. and Aalberts, D.P. (2022) The Four mRNA Bases Have Quite Different (Un)folding Free Energies, Applications to RNA Splicing and Translation Initiation with BindOligoNet. *Journal of Molecular Biology*, **434**, 167578.

86. Moore, S.J., MacDonald, J.T., Wienecke, S., Ishwarbhai, A., Tsipa, A., Aw, R., Kylilis, N., Bell, D.J., McClymont, D.W., Jensen, K. *et al.* (2018) Rapid acquisition and model-based analysis of cell-free transcription-translation reactions from nonmodel bacteria. *Proceedings of the National Academy of Sciences of the United States of America*, **115**, E4340-E4349.

87. Iost, I., Guillerez, J. and Dreyfus, M. (1992) Bacteriophage T7 RNA polymerase travels far ahead of ribosomes in vivo. *Journal of bacteriology*, **174**, 619-622.

88. Goyal, A., Belardinelli, R., Maracci, C., Milón, P. and Rodnina, M.V. (2015) Directional transition from initiation to elongation in bacterial translation. *Nucleic acids research*, **43**, 10700-10712.

89. Huch, S., Nersisyan, L., Ropat, M., Barrett, D., Wu, M., Wang, J., Valeriano, V.D., Vardazaryan, N., Huerta-Cepas, J., Wei, W. *et al.* (2023) Atlas of mRNA translation and decay for bacteria. *Nature microbiology*, **8**, 1123-1136.

90. Chen, H., Shiroguchi, K., Ge, H. and Xie, X.S. (2015) Genome-wide study of mRNA degradation and transcript elongation in Escherichia coli. *Molecular systems biology*, **11**, 781.

91. Celesnik, H., Deana, A. and Belasco, J.G. (2007) Initiation of RNA decay in Escherichia coli by 5' pyrophosphate removal. *Molecular cell*, **27**, 79-90.

92. Deana, A., Celesnik, H. and Belasco, J.G. (2008) The bacterial enzyme RppH triggers messenger RNA degradation by 5′ pyrophosphate removal. *Nature*, **451**, 355-358.

93. Mackie, G.A. (2013) RNase E: at the interface of bacterial RNA processing and decay. *Nature Reviews Microbiology*, **11**, 45-57.

94. Richards, J. and Belasco, J.G. (2023) Graded impact of obstacle size on scanning by RNase E. *Nucleic acids research*, **51**, 1364-1374.

95. Castillo-Mendez, M.A., Jacinto-Loeza, E., Olivares-Trejo, J.J., Guarneros-Pena, G. and Hernandez-Sanchez, J. (2012) Adenine-containing codons enhance protein synthesis by promoting mRNA binding to ribosomal 30S subunits provided that specific tRNAs are not exhausted. *Biochimie*, **94**, 662-672.

Table

Table 1: Oligonucleotides
Sequences in bold are homologous to the plasmid backbone, while sequences underlined contain the modifications in the first codon of the *yfp* or the MGapt aptamer.

No.	Sequence (5'→3')	Purpose
Amplification of the plasmid backbone		
P005-F	AAGTAA**TAATTCGAGCTCGG**	Amplification of pMMB67EH for cloning of all variants
P006-R	*GATTTTGGACAT***ATTCTGTTTCCTGTG**	Amplification of pMMB67EH for cloning of TBT, TBT_{K3E}, TBT_{K3L}, TBT_{K6L}, TBT_{K6E}
P029-R	CAT**ATTCTGTTTCCTGTGTG**	Amplification of pMMB67EH for cloning of YFP, YFP_M, YFP_A, TBT_G, YFP_{StoK}, YFP_{E6K}, YFP_{E6-7K}
C082-F	**CTCGAGCACCACCACC**	Amplification of pET21 for cloning of all variants
C081-R	GATTTTTACGATTTTGGA**CAT**ATGTATATCT	Amplification of pET21 with insertion of TBT sequence
Amplification of the *yfp* part		
P008-R	**CGAGCTCGAATTA**TTACTTGTACAGC	Reverse amplification of all YFP variants
P032-F	**CACAGGAAACAGAAT**ATGGTGAGCAAGGGC	Amplification of YFP
C018-F	**CAGGAAACAGAAT**ATGGTAAGTAAAGGAGAAGAACT GTTCACCGGGGTG	Amplification of YFP_A
C019-F	**CAGGAAACAGAAT**ATGGTATCAAAGGGTGAAGAACT GTTCACCGGGGTG	Amplification of YFP_M
E022-F	**CAGGAAACAGAAT**ATGGTGAGCAAGGGCAAAGAGCT GTTCACCGGGGTG	Amplification of YFP_{E6K}
E023-F	**CAGGAAACAGAAT**ATGGTGAGCAAGGGCAAAAAACT GTTCACCGGGGTG	Amplification of YFP_{E6-7K}
E078-F	**CAGGAAACAGAAT**ATGGTGAAGAGCGGCGAGGAGC TGTTCACCGGGGTG	Amplification of YFP_{StoK}
P007-F	AAT*ATGTCCAAAATCGTAAAAATC*GTGAGCAAGGGCG AGG	Amplification of TBT
C021-F	**CAGGAAACAGAAT**ATGTCGAAGATCGTGAAGATCGT GAGCAAGGGCGAGGAG	Amplification of TBT_G
E024-F	AATATGTCCTTAATCGTAAAAATCGTGAGCAAGGGCG AGG	Amplification of TBT_{K3L}
E025-F	AATATGTCCGAAATCGTAAAAATCGTGAGCAAGGGCG AGG	Amplification of TBT_{K3E}
E079-F	AATATGTCCAAAATCGTATTAATCGTGAGCAAGGGCG AGG	Amplification of TBT_{K6L}
E080-F	AATATGTCCAAAATCGTAGAAATCGTGAGCAAGGGCG AGG	Amplification of TBT_{K6E}
Amplification of the test genes for TBT sequence insertion		
C083-F	CAAAATCGTAAAAATCTCGCTGCCGCACCTC	Amplification *ycaQ* in pET21 with TBT sequence
C084-R	GGTGGTGGTGCTCGAGTGCGACGGGGTCTATTTC	
C085-F	CAAAATCGTAAAAATCGCGCGTTCGATCGAT	

C086-R	GGTGGTGGTGCTCGAGCTTGCGGAACTTGTC	Amplification RSP_2139 in pET21 with TBT sequence
C087-F	CAAAATCGTAAAAATCAGCACGCGGACGAGG	Amplification SCO1897 in pET21 with TBT sequence
C088-R	GGTGGTGGTGCTCGAGGACGCGGATGATCT	
C089-F	CAAAATCGTAAAAATCGCCGCCATGCCCAAGC	Amplification SRU_1983 in pET21 with TBT sequence
`	GGTGGTGGTGCTCGAGCGAGGTGGACGGCCG	

Amplification for insertion of the MGapt aptamer

H070-R	GATCCATTCGTTACCTGGCTCTCGCCAGTCGGGATCCCGCTCGAATTATTACTTGTACAGC	Insertion of the MGapt in TBT and TBT_G constructs
H071-F	AGCCAGGTAACGAATGGATCTCGGTACCCGGGGATCC	

Sequencing

P031-F	CTGAAATGAGCTGTTGAC	Sequencing of pMMB67EH
P010-R	TGCCTGCAGGTCGACT	
C093-F	GCGATATAGGCGCCAGC	Sequencing of pET21
C094-R	TTCAGCAAAAAACCCCTCAAGAC	

DNA probe for northern blot

D072	CAGCCAAGCTTGCATGCCTGCAGGTCGACTCTAGAGGATCCCCGGG	3'UTR of *yfp* transcripts DNA probe
C045	CGTCCTTCATCGCCTCTGACT	DNA 23S probe

***In vitro* transcription template**

C034	GCGAATTAATACGACTCACTATAGGAATTGTGAGCGGATAACAATTTCACAC	Amplification of fragment for T7 *in vitro* transcription
C035	CCGACAAACAACAGATAAAACGAAAG	

Figure 1

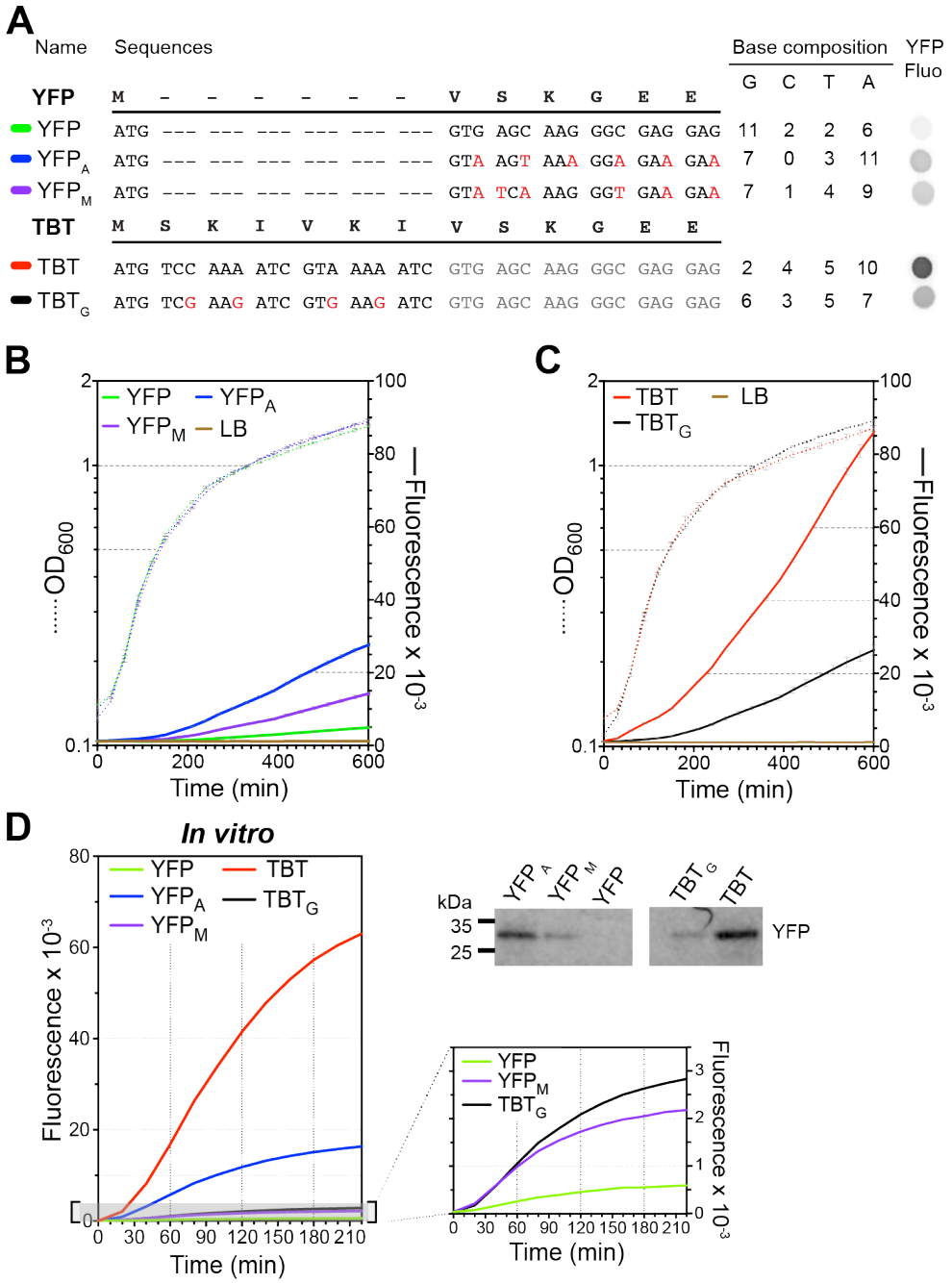

Figure 2

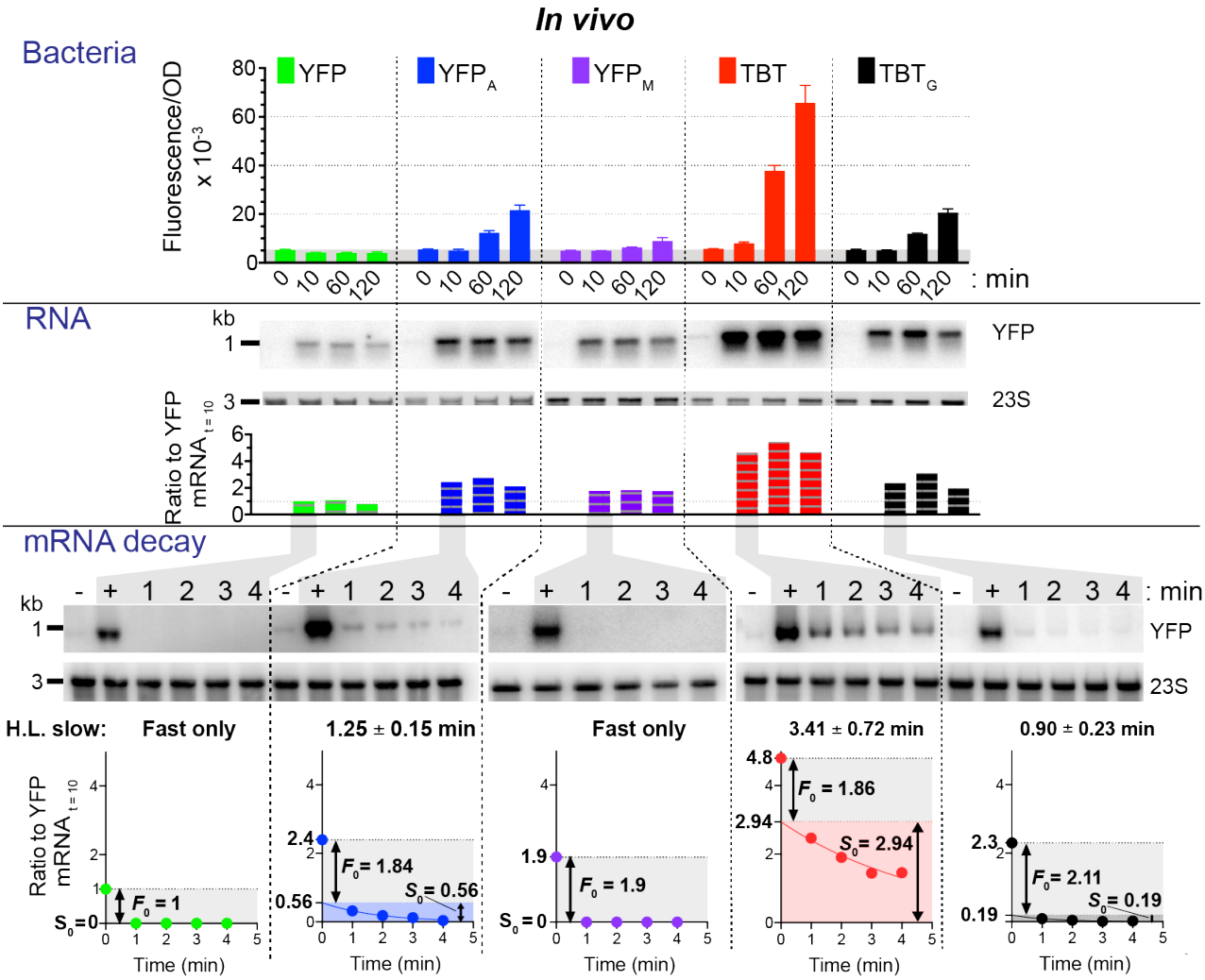

Figure 3

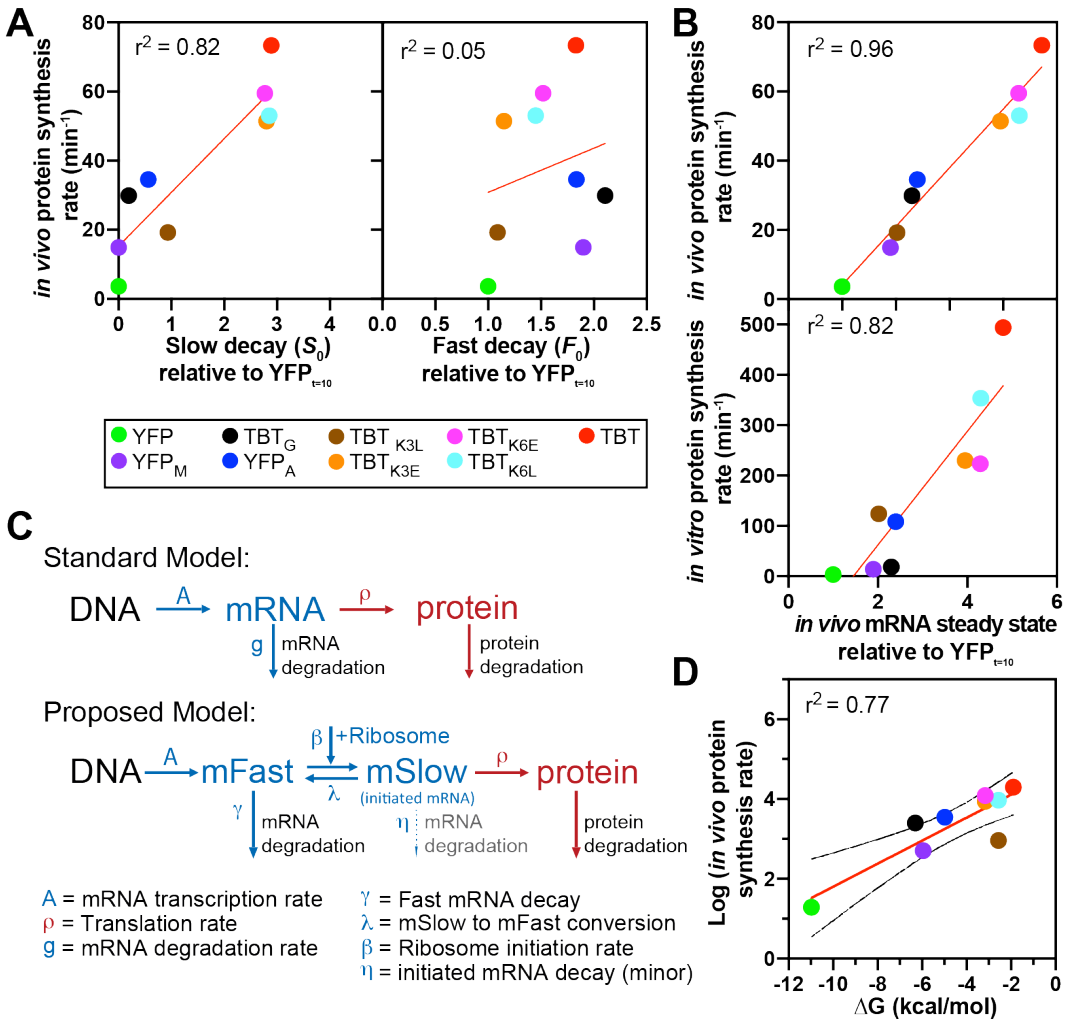

Figure 4

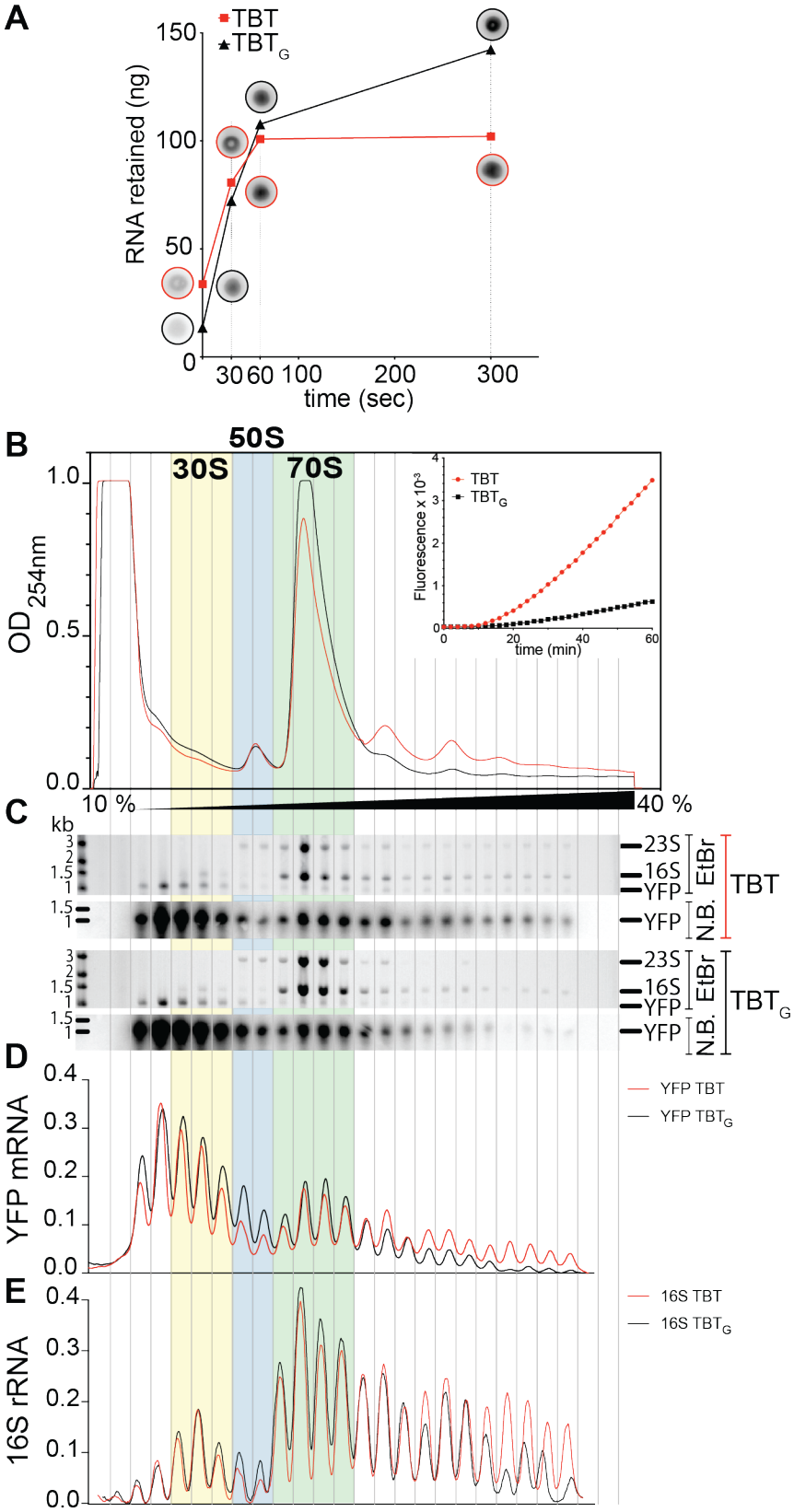

Figure 5

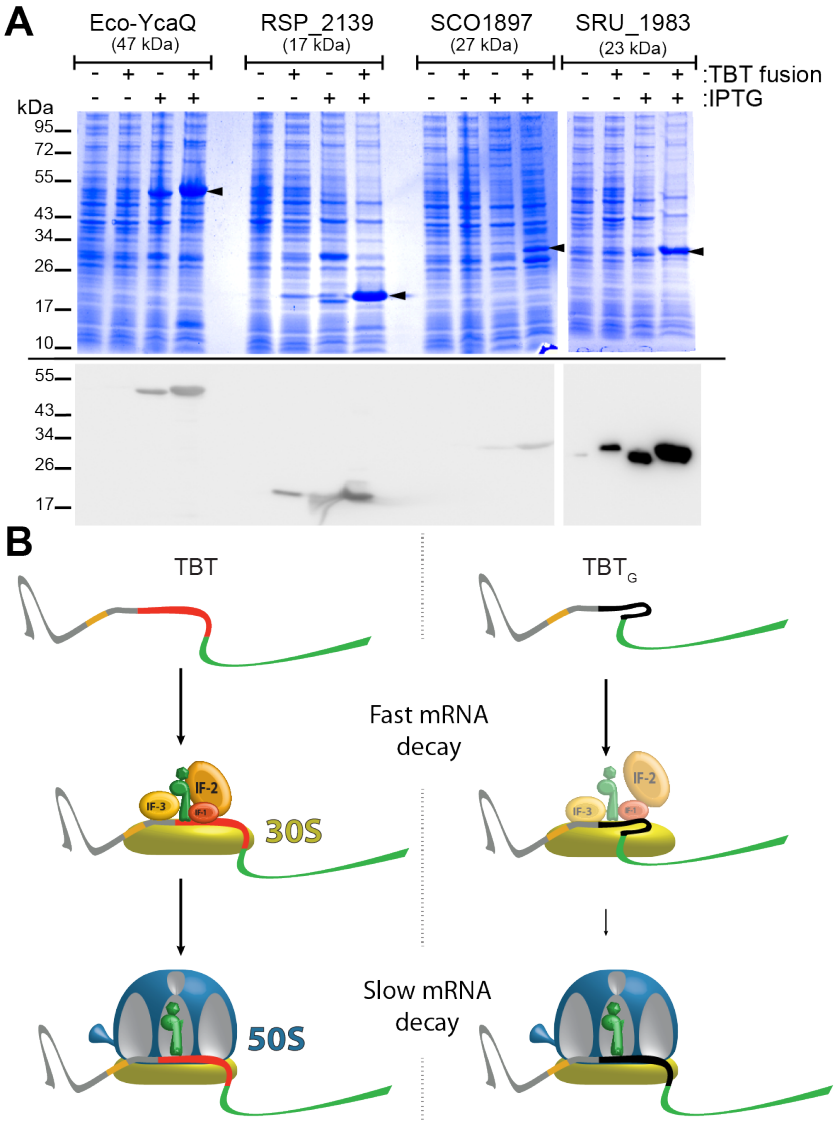

Figure legends:

Figure 1: Influence of A-richness in initial codons on protein expression. A) Sequences of YFP constructs with synonymous codon replacements in the first 7 codons (YFP_A, highest A content; YFP_M, using our model M optimal tail codons(13)). Below, YFP constructs with TBT sequence added at the 5' end and TBT sequence with replacement by synonymous codons rich in G (TBT_G). Right, base composition of the constructs and drop assay of different variants, showing the different level of fluorescence *in vivo* on solid medium. **B and C)** *In vitro* measurement of growth and fluorescence of *E. coli* performed in 96-well plate, in LB medium in presence of 1 mM IPTG, **B)** for the YFP and **C)** for the TBT variants. **D)** Fluorescence signal of *in vivo* translation for YFP and TBT variants (PureExpress translation assay with a final concentration of 1.4 µM for each mRNA). Top right, western blots of the final translation reactions revealed with an anti-GFP antibody.

Figure 2: Influence of A-richness on mRNA stability. Fluorescence levels of culture of the different variants collected 10 min, 60 min and 120 min after induction at OD_{600}=0.5. Below, northern blotting of total RNA from the corresponding cultures using a DNA probe that hybridizes with the 3'UTR of the *yfp* mRNA. The level of 23S rRNA is showed beneath the northern blot. In the lower section, a mRNA stability test is presented. Northern blot of total RNA isolated from the same strains using the same induction procedure as above. Transcription was halted by rifampicin addition, and samples were collected before induction (-), after 10 min induction (+), and at 1, 2, 3, and 4 min after rifampicin addition. Below, quantification of the northern blot signal normalized to the *yfp* mRNA signal at 10 min after induction along with curve fitting of the decay to an exponential decay for the slow decay part of the kinetic. The proportion of Fast decay (F_0) and Slow decay (S_0) is indicated and the rate of the S_0 decay is indicated above the graph.

Figure 3: The change in mRNA stability is governed by the ribosome. A) The *in vivo* fluorescence increase correlated with the S_0 or F_0 populations (normalized on the *yfp* mRNA signal at 10 min after induction). **B**) Correlation of the *in vivo* or *in vitro* fluorescence increase with the *yfp* mRNA signal at 10 min after induction (normalized on the *yfp* mRNA signal). **C**) Standard model of mRNA decay and our proposed model including the various variables used to construct the model. **D**) Correlation of the logarithm of the *in vivo* fluorescence increase with the energy of folding (ΔG) of the first 21 nucleotides calculated using the BindOligoNet G_5 model(85). In **A**, **B**, **D** the red line is the linear regression, the r^2 of the goodness of the fit is reported in the right left corner of each graph. In **D** the doted lines show the error.

Figure 4: Change in A content for the TBT construct affects the formation of the 70S IC ribosome but not its affinity for the 30S subunit. **A**) Filter binding assay of the P^{32}-labeled mRNA (TBT or TBT_G), quantified after different incubation time with the 30S ribosomal subunit. Image filter after scanning are presented in the circles. **B**) Polysomes separation and fractionation of IVTA programed with the TBT or TBT_G mRNAs after 1 h of incubation (the IVTA is presented in the insert). **C**) Ethidium bromide stained gel (EtBr) or northern blot (N.B.) of the total RNA purified from each fraction of the polysome profiles. **D**) Normalized graph of the quantification of the northern blot signal for the TBT or TBT_G mRNAs. **E**) Normalized graph of the quantification of the Ethidium bromide stained gel signal for the 16S rRNA.

Figure 5: Use of the TBT sequence to improve protein expression and model of its effect on translation initiation and mRNA decay. **A**) SDS-PAGE showing induction or not of tested proteins (black arrows) with their WT sequence or the sequences with the TBT sequence fused in N-terminal. Protein induction was performed as previously(13) the in *E. coli* Bl21 DE3 strain with 1 mM IPTG for 16 h at 17 °C. Below, Western Blot with anti-his antibodies showing induction of tested proteins. **B**) Model illustrating the impact of A-richness in initial codons, derived from observations of TBT vs. TBT_G. The TBT mRNA rapidly assembles into a 70S initiation complex (IC), whereas the TBT_G mRNA exhibits slower 70S IC formation, getting trapped at the 30S IC formation stage. It remains uncertain whether the kinetic restriction occurs before or after the assembly of initiation factors and the initiator fMet-$tRNA^{fMet}$. The free pool of mRNA and the stalled 30S IC or pre-30S IC with the TBT_G construct undergo rapid degradation, while the mRNAs engaged in the 70S IC are stabilized, leading to a slower decay.